

Article

Enhancing Sensitivity of Double-Walled Carbon Nanotubes with Longitudinal Magnetic Field

Hamid Reza Ahmadi ¹, Zaher Rahimi ^{2,*} and Wojciech Sumelka ^{3,*} 

¹ Mechanical Engineering Department, Urmia University, Urmia 5714783734, Iran; ahmadi.hamidreza.mechanic@gmail.com

² School of Engineering and Technology, University of New South Wales, Canberra, ACT 2600, Australia

³ Institute of Structural Analysis, Poznan University of Technology, 60-965 Poznan, Poland

* Correspondence: sayed_ramyar.rahimi@unsw.edu.au (Z.R.); wojciech.sumelka@put.poznan.pl (W.S.)

Abstract: In this study, the behavior of double-walled carbon nanotubes (DWCNTs) used as mass sensors is explored under various boundary conditions; particular attention is paid to the crucial topic of resonant nanomechanical mass sensors. In the presented approach, nanotubes are subjected to a distributed transverse magnetic force and supported by an elastic foundation. The impacts of the longitudinal magnetic field, elastic medium, and diverse physical parameters on the responsiveness of the sensors are assessed. Using the energy method, governing equations are formulated to determine the frequency shifts of the mass nanosensors. Our findings reveal significant variations in the frequency shifts due to a longitudinal magnetic field, which depends on the applied boundary conditions. This research holds significance in the design of resonant nanomechanical mass sensors and provides valuable insights into the interplay of factors affecting their performance. Through exploring the intricate dynamics of DWCNTs used as mass sensors and thus contributing to the broader understanding of nanoscale systems, the implications for advancements in sensor design are offered and applications are introduced.

Keywords: nanoresonators; mass sensor; magnetic field; double-walled carbon nanotube; frequency shift



Citation: Ahmadi, H.R.; Rahimi, Z.; Sumelka, W. Enhancing Sensitivity of Double-Walled Carbon Nanotubes with Longitudinal Magnetic Field. *Appl. Sci.* **2024**, *14*, 3010. <https://doi.org/10.3390/app14073010>

Academic Editors: Antonio Miotello and Gregory Slepyan

Received: 31 October 2023

Revised: 22 February 2024

Accepted: 25 March 2024

Published: 3 April 2024



Copyright: © 2024 by the authors. Licensee MDPI, Basel, Switzerland. This article is an open access article distributed under the terms and conditions of the Creative Commons Attribution (CC BY) license (<https://creativecommons.org/licenses/by/4.0/>).

1. Introduction

The advent of carbon nanotubes has created a new revolution in engineering sciences and medical technology. Carbon nanotubes (CNTs) are essential in improving the functioning of nanodevices, such as nanoelectromechanical system (NEMS) nanoresonators and sensors [1]. CNT-based nanosensors have been used extensively in different applications, such as ultrasensitive mass and force sensing, cooling and quantum measurement, and chemical and biological sensing, to detect the masses of bacteria, cells, and viruses [2–5]. In the case of mass detection, two methods (static and dynamic) are typically used to detect added mass in nano-mass sensors [6–8].

In the static method, the added mass is determined by measuring the deflection of a nano-beam resulting from the attached mass on the surface. The dynamic method analyzes the shift in the system's frequency due to the attached mass [9]. A higher frequency shift shows the superior sensitivity of a mass sensor [10], which is affected by various parameters, such as geometry [11], vibration modes [12], the characteristics of the structure [13], and surface functionalization [14]. Additionally, external parameters, such as temperature and environmental conditions, can affect the performance of nano-mass sensors [15]. Research has been conducted to enhance and assess the sensitivity of mass nanosensors and has primarily been driven by these factors. Chowdhury et al. [6] conducted a study on carbon nanotube-based biosensors in which they proposed a straightforward analytical relationship using a linear approximation of the non-linear sensor equation. Their approach aimed to detect the masses of biological samples through the analysis of frequency shifts in both

cantilevered and bridged carbon nanotubes. Zarepour et al. [16] studied the transverse vibrations of supported and bridged nano-beams, which had attached masses and rotational and transverse springs at their ends. The effects of the geometric parameters of mechanical elements were also considered by Ardali et al. [11]; in particular, they investigated the impacts of the various geometric parameters of microbeams on mass sensors and realized that the sensitivity of a microsensor increases with microbeam rigidity. In another work, Bouchaala et al. [17] compared micro-CNTs and beam mass sensors and found that the CNT-based sensor was more sensitive than the microbeam sensor. Habibi et al. [18] studied the position and mass identification in a single-walled carbon nanotube (SWCNT) mass sensor. Soltani et al. [19] investigated the sensitivity of an SWCNT mass sensor resting on an elastic foundation using non-local elasticity theory and proposed the parametric study of elastic foundation parameters. Patel et al. [20] analyzed the vibrations of DWCNTs to sense biological objects, considering six different types of DWCNTs to determine the best type for mass sensors. They concluded that cantilevered configurations were four times more sensitive than bridged configurations.

As enhancing the sensitivity of mass sensors is necessary to measure smaller masses, which is necessary in the fields of biotechnology and life sciences, higher mass sensitivity facilitates the detection of molecular interactions and biomolecular events with greater precision [21]. Therefore, researchers have tried to enhance the sensitivity of current mass sensors through the application of modifications or the introduction of new methods. For example, Ghatkesar et al. [22] used a system of gold layers of varying thicknesses and showed a linear increase in mass sensitivity using higher vibration modes. They concluded that the sensitivity experiences an enhancement of two orders of magnitude when transitioning from mode 1 to mode 7. Saiz et al. [23] investigated a new way to increase the mass sensitivity of a magnetoelastic resonator. They theoretically and experimentally showed that, through tailoring the sensor geometry and mass load position, a mass sensitivity enhancement exceeding 400% was noted in a magnetoelastic sensor with the utilization of novel sensor platform geometries. Gil-Santos et al. [12] proposed a novel approach to mass sensing and stiffness spectroscopy, focusing on the phenomenon whereby a nanoresonator enters a superposition state characterized by two orthogonal vibrations with distinct frequencies upon the disruption of symmetry. The measurement of these frequencies enables the determination of the mass, stiffness, and azimuthal arrival direction of the adsorbate. In the current research, we focus on how it is possible to increase the frequency shift—and, consequently, to enhance sensitivity—through the use of a longitudinal magnetic field [10].

The applications of magnetic fields in micro- and nanoelectromechanical systems have been addressed in many studies [24–26]. In the case of sensors, coupling the magnetic effect with acoustic resonator sensors offers significant advantages and the possibility to use a much wider variety of materials for the transducers, when compared to piezoelectric resonators, allowing more flexibility and a potentially improved performance. This approach was used by Lucklum et al. [27] to detect fluid volumes, liquid viscosity, and density. Moreover, the influence of magnetic forces on the behavior of micro- and nanomechanical elements has been extensively investigated as an external parameter. Murmu et al. [28] demonstrated that the frequencies of a DWCNT increase with an increase in the magnetic field. They also investigated the effect of a longitudinal magnetic field on the transverse vibration of a magnetically sensitive material. Sobamowo et al. [29] conducted a comprehensive parametric study on multi-walled carbon nanotubes in a magneto-thermal environment. Their study considered the nanotube geometry and explored other parameters, such as the number of walls, initial curvature, and environmental factors, including the temperature and magnetic field. Zhang et al. [30] showed the effect of the strength of the magnetic field on the vibration of an SWCNT embedded in a viscoelastic medium. They proposed a new analytical expression for the complex natural frequencies for certain typical boundary conditions and the Kelvin–Voigt model and demonstrated the efficiency of their proposed methods in the vibration analysis of embedded SWCNTs under a magnetic field. Sadeghi-Goughari et al. [31] analyzed the vibrational behavior of a CNT conveying a

nanoflow subjected to a longitudinal magnetic field. Zhen et al. [32] explored the longitudinal magnetic field's influences on the vibration of viscoelastic nanotubes based on the non-local strain gradient Timoshenko beam model. Yinusa et al. [33] investigated the effect of an external magnetic field on the nonlinear vibration of a CNT conveying a fluid. Their study revealed that the magnetic term significantly attenuated or dampened the system's vibration by approximately 20%.

Moreover, in the case of modeling improvement, Arda and Aydogdu [34] recently focused on both the inertia and stiffness of the detected mass by considering it as an elastic body with stiffness. Their findings showed that including the stiffness of the detected mass introduced an additional frequency to the spectrum of the nano-beam, resulting in a shift in the nano-beam's frequencies to the adjacent higher mode. Furthermore, Ceballes et al. [35] employed the Timoshenko beam theory and Eringen's non-local theory of elasticity to enhance the modeling accuracy, particularly for short beams. They found that the Euler-Bernoulli beam theory overpredicted the frequency shift, compared to the Timoshenko beam theory. Overall, the sensitivity of resonant mass sensors relies significantly on the effective vibratory mass. This is influenced by both the geometry and configuration of the resonant structure and the properties of the materials that make up the structure [36]. In this research, the effect of changing the configuration of the resonant structure is studied by considering the mass sensor inside a longitudinal magnetic field.

In nanoscale mechanics modeling, small-scale effects are crucial in accurately describing the mechanical behavior of nanostructures. At the nanoscale, material properties and structural dimensions deviate from those observed in the macroscopic world [37]. Several theories have been proposed to address these nonclassical phenomena, including Eringen's non-local theory, the modified couple stress theory, and nonclassical fractional-based theories [38–41]. These theories consider the influences of size and surface effects on the mechanical responses of nanostructures. Among these approaches, Eringen's non-local theory has gained significant popularity. It introduces a non-local parameter for the influence of neighboring atoms or molecules on a material's mechanical behavior. The non-local theory has been successfully applied to various problems [42–46]. Its ability to accurately capture the size-dependent behavior of nanostructures makes it a valuable tool in the analysis and design of nanoscale systems.

This study investigates the sensitivity of biosensors based on DWCNTs subjected to a longitudinal magnetic field. In contrast to SWCNTs, DWCNTs demonstrate superior thermal and chemical stability. They have been applied in various fields, such as those using gas sensors, dielectric devices, nanoelectronic devices, nanocomposites, emitters, and others. The synthetic combination of single-walled, multi-walled, and double-walled carbon nanotubes showcases the electrical and thermal stability of the latter and the flexibility of the former. Meanwhile, using a longitudinal magnetic field is intended to enhance the sensitivity and performance of DWCNT-based biosensors [47–50]. Additionally, in the case of sensitivity, non-SWCNTs are much easier to manipulate [10,51]. Therefore, in the current research, the vibrating behavior of DWCNTs resting on an elastic foundation and subjected to a longitudinal magnetic field is investigated through the derivation of the governing equations using Eringen's non-local theory. The Lorentz magnetic force is considered and is obtained from Maxwell's relation. The effects of the longitudinal magnetic field are analyzed for three different sensor configurations: simply supported, cantilevered, and bridged. Through studying these effects, this research contributes to the advancement and design of mass sensors utilizing DWCNTs in a longitudinal magnetic field. This study might provide deeper insights into further developments in mass sensing and the application of DWCNT-based sensors.

2. Theoretical Basis

A schematic diagram of a simply supported DWCNT beam embedded in an elastic foundation, subjected to an external force (F_{ext}), and carrying an attached concentrated mass (m_c) along its length position ($x = a$) is shown in Figure 1. In this paper, the non-

local Euler–Bernoulli beam model is applied to study the free vibration of a DWCNT. The governing equations of a viscoelastic nano-beam under a longitudinal magnetic field based on non-local elasticity theory can be obtained as follows [43]:

$$EI \frac{\partial^4 w(x,t)}{\partial x^4} + \rho A \frac{\partial^2 w(x,t)}{\partial t^2} - (e_0 a)^2 \left(\rho A \frac{\partial^4 w(x,t)}{\partial x^2 \partial t^2} - \frac{\partial^2 F_{ext}(x,t)}{\partial x^2} \right) = F_{ext}(x,t), \quad (1)$$

where e_0 is a constant for calibrating the model using experimental results and other validated models and a is the length of the internal characteristics. The external force (F_{ext}) is a combination of several factors acting on the nanotube, including the forces per unit length induced by the magnetic field (q_{mag}), the Winkler foundation force ($q_{elastic\ medium}$), and the force of the interaction between the inner and outer nanotubes (q_{van}), which can be expressed as follows:

$$F_{ext} = q_{mag} + q_{elastic\ medium} + q_{van}. \quad (2)$$

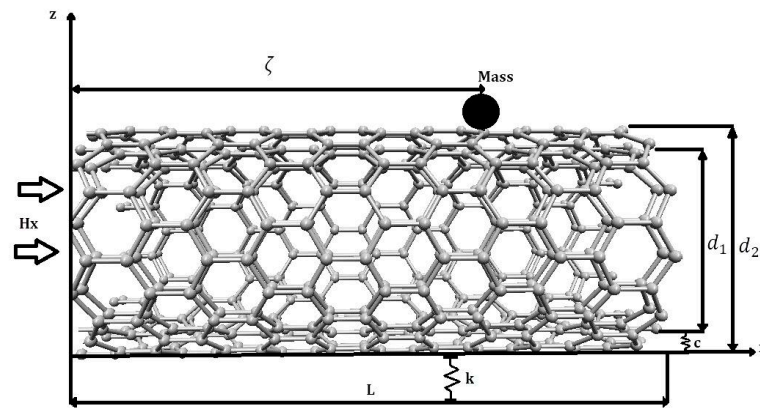


Figure 1. Schematic diagram of the DWCNT with attached mass under a longitudinal magnetic field.

Maxwell's Relations

When applying a longitudinal magnetic field vector ($\bar{H}(H_x, 0, 0)$), a Lorentz force acts on the DWCNT. For the present study, $w = w(x, t)$; so, the Lorentz force in the z direction is written as follows:

$$F_z = \eta H_x^2 \left(\frac{\partial^2 w(x,t)}{\partial x^2} \right), \quad (3)$$

where η is the magnetic field permeability and H_x denotes the magnetic intensity of the longitudinal magnetic field. Therefore, the pressure exerted on the nanotube due to a Lorentz magnetic field can be expressed as follows:

$$q_{mag} = \int_A F_z dz = \eta A H_x^2 \left(\frac{\partial^2 w(x,t)}{\partial x^2} \right). \quad (4)$$

As shown in Figure 1, the interaction between the inner and outer nanotubes is facilitated by van der Waals forces and can be obtained as follows:

$$q_{van} = c(w_2 - w_1). \quad (5)$$

The subscripts 1 and 2 denote the inner and outer nanotubes, respectively; furthermore, c is the van der Waals interaction coefficient, which is written as follows [28,52]:

$$c = \frac{320 \times 2R_1}{0.16a^2}, \quad (a = 0.142 \text{ nm}), \quad (6)$$

where R_1 is the internal diameter of the nanotube. The Winkler foundation model describes the effect of the elastic medium on the outer nanotube. Therefore, for a DWCNT with transverse displacement in the z direction, we have

$$q_{elastic\ medium} = kw_2, \tag{7}$$

where k is the elastic foundation modulus.

Substituting Equations (4), (5) and (7) into Equation (2) and substituting the result into Equation (1), one obtains the equation of motion for the inner nanotube:

$$EI_1 \frac{\partial^4 w_1}{\partial x^4} - (e_0 a)^2 \left(\rho A_1 \frac{\partial^4 w_1}{\partial x^2 \partial t^2} - \eta A_1 H_x^2 \frac{\partial^4 w_1}{\partial x^4} + c \frac{\partial^2 w_1}{\partial x^2} - c \frac{\partial^2 w_2}{\partial x^2} \right) + \rho A_1 \frac{\partial^2 w_1}{\partial t^2} - \eta A_1 H_x^2 \frac{\partial^2 w_1}{\partial x^2} = c(w_2 - w_1). \tag{8}$$

The equation for the outer nanotube is as follows:

$$EI_2 \frac{\partial^4 w_2}{\partial x^4} - (e_0 a)^2 \left(\rho A_2 \frac{\partial^4 w_2}{\partial x^2 \partial t^2} + M(\delta(x - \zeta)) \frac{\partial^4 w_2}{\partial x^2 \partial t^2} - \eta A_2 H_x^2 \frac{\partial^4 w_2}{\partial x^4} - c \frac{\partial^2 w_1}{\partial x^2} + c \frac{\partial^2 w_2}{\partial x^2} \right) - \eta A_2 H_x^2 \frac{\partial^2 w_2}{\partial x^2} + [\rho A_2 + M(\delta(x - \zeta))] \frac{\partial^2 w_2}{\partial t^2} + kw_2 = c(w_1 - w_2). \tag{9}$$

Assuming the motion is harmonic, an approximate solution for Equations (8) and (9) is obtained using the Galerkin approximation. Thus, the transverse deformation of each point on the inner and outer nanotubes can be expressed as follows:

$$w_1(x, t) = \sum_{n=1}^N \phi_{1n}(x) e^{i\omega_n t}, w_2(x, t) = \sum_{n=1}^N \phi_{2n}(x) e^{i\omega_n t}, \tag{10}$$

where ω_n denotes the natural frequency of the DWCNT and $\phi_n(x)$ are the eigenfunctions, which depend on the beam-end condition. For the n th vibration mode and simply supported beam conditions, $\phi_{1n}(x) = \phi_{2n}(x) = \sin \frac{n\pi x}{l}$. Next, for the n th vibration mode of a cantilevered DWCNT,

$$\phi_n(x) = \left(\cosh(z_n \frac{x}{l}) - \cos(z_n \frac{x}{l}) \right) - \left(\sinh(z_n \frac{x}{l}) - \sin(z_n \frac{x}{l}) \right) \times \left(\frac{\sin h z_n - \sin z_n}{\cosh z_n + \cos z_n} \right). \tag{11}$$

Finally, for the n th vibration mode of a bridged DWCNT,

$$\phi_n(x) = \left(\cosh z_n \frac{x}{l} - \cos z_n \frac{x}{l} \right) - \left(\sinh z_n \frac{x}{l} - \sin z_n \frac{x}{l} \right) \times \left(\frac{\cosh z_n + \cos z_n}{\sin h z_n - \sin z_n} \right) \tag{12}$$

where z_n are the roots of the following equation. The natural frequency of a cantilevered DWCNT is also related to the z_n :

$$\cosh(z_n) \cos(z_n) = 1. \tag{13}$$

As mentioned in the introduction, the energy method is employed to determine the natural frequency of a cantilevered DWCNT and the frequency shift due to added mass. Therefore, the kinetic energy of the inner-walled DWCNT can be obtained as follows [20,53]:

$$T_1 = \frac{\omega^2}{2} \int_0^l \rho A_1 \left((\phi_{1n}(x))^2 - (e_0 a)^2 \left[\frac{\partial \phi_{1n}(x)}{\partial x} \right]^2 \right) dx. \tag{14}$$

The kinetic energy of the outer-walled DWCNT can be obtained as

$$T_2 = \frac{\omega^2}{2} \left(\int_0^l \rho A_2 \left((\phi_{2n}(x))^2 - (e_0 a)^2 \left[\frac{\partial \phi_{2n}(x)}{\partial x} \right]^2 \right) dx + M \left((\phi_{2n}(\zeta))^2 - (e_0 a)^2 \left[\frac{\partial^2 \phi_{2n}(x)}{\partial x^2} \right]^2 \right) \right). \tag{15}$$

The total kinetic energy of a DWCNT is the sum of the kinetic energies of the inner and outer nanotubes. Therefore,

$$T_t = T_1 + T_2. \tag{16}$$

According to the kinetic energy equivalence and the position of the mass particle in the middle of the cantilevered beam, substituting Equations (15) and (16) into (17), we obtain

$$m_{eq} = \rho \left(l(A_1 + A_2) - (e_0a)^2 \left(\int_0^l \left(A_1 \left[\frac{\partial \varphi_{1n}(x)}{\partial x} \right]^2 + A_2 \left[\frac{\partial \varphi_{2n}(x)}{\partial x} \right]^2 \right) dx \right) \right) + M \left((\varphi_{2n}(\zeta))^2 - (e_0a)^2 \left[\frac{\partial^2 \varphi_{2n}(x)}{\partial x^2} \Big|_{\zeta} \right]^2 \right). \tag{17}$$

Next, the potential energy of the inner-walled DWCNT can be obtained as follows [20]:

$$P_1 = \frac{1}{2} \left(EI_1 + (e_0a)^2 \eta A_1 H_x^2 \right) \int_0^l \left[\frac{\partial^2 \varphi_{1n}(x)}{\partial x^2} \right]^2 dx + \frac{1}{2} c (e_0a)^2 \int_0^l \left[\frac{\partial \varphi_{2m}(x)}{\partial x} \right]^2 dx - \frac{1}{2} \left(c (e_0a)^2 \int_0^l \left[\frac{\partial \varphi_{1m}(x)}{\partial x} \right]^2 dx + \eta A_1 H_x^2 \right) \int_0^l \left[\frac{\partial \varphi_{1n}(x)}{\partial x} \right]^2 dx + \frac{1}{2} \int_0^l c [\varphi_{1m}(x)]^2 dx - \frac{1}{2} \int_0^l c [\varphi_{2m}(x)]^2 dx. \tag{18}$$

Meanwhile, the potential energy of the outer-walled DWCNT is

$$P_2 = \frac{1}{2} \left(EI_2 + (e_0a)^2 \eta A_2 H_x^2 \right) \int_0^l \left[\frac{\partial^2 \varphi_{2n}(x)}{\partial x^2} \right]^2 dx + \frac{1}{2} \int_0^l c [\varphi_{2n}(x)]^2 dx - \frac{1}{2} \int_0^l c [\varphi_{1n}(x)]^2 dx - \frac{1}{2} \left((c + k) (e_0a)^2 + \eta A_2 H_x^2 \right) \int_0^l \left[\frac{\partial \varphi_{2n}(x)}{\partial x} \right]^2 dx + \frac{1}{2} (e_0a)^2 \int_0^l c \left[\frac{\partial \varphi_{1n}(x)}{\partial x} \right]^2 dx + \frac{1}{2} \int_0^l k [\varphi_{2n}(x)]^2 dx. \tag{19}$$

Hence, the total potential energy of the DWCNT is the sum of the potential energies of the inner and outer nanotubes. Therefore,

$$P_t = P_1 + P_2. \tag{20}$$

Finally, according to the potential energy equivalences, through substituting Equations (19) and (20) into (21) we obtain

$$k_{eq} = \frac{z_n^4}{l^3} \left[EI_1 + EI_2 + (e_0a)^2 \eta H_x^2 (A_2 + A_1) \right] - \frac{z_n^2}{l} \left(\eta H_x^2 (A_2 + A_1) - k (e_0a)^2 \right) + kl + c(\zeta_{1m} - \zeta_{1n}) + c(\zeta_{2n} - \zeta_{2m}) - c(e_0a)^2 (\xi_{1m} - \xi_{1n}) + c(\xi_{2n} - \xi_{2m}). \tag{21}$$

Due to the boundary condition of the cantilevered DWCNT and the location of the absorbed mass, the fundamental resonant frequency is

$$f_n = \frac{1}{2\pi} \sqrt{\frac{k_{eq}}{m_{eq}}}. \tag{22}$$

The resultant frequency of the DWCNT without the attached mass is

$$f_{on} = \frac{1}{2\pi} \sqrt{\frac{k_{eq}}{\rho l (A_1 + A_2)}}. \tag{23}$$

Using Equations (22) and (23), the frequency shift can be expressed as follows:

$$\Delta f = f_{on} - f_n = f_{on} - \frac{f_{on}}{\sqrt{1 + \beta_m M}}, \tag{24}$$

where $\beta_m = \frac{\varphi_n(\zeta) \varphi_m(\zeta)}{\rho l (A_1 + A_2)}$.

Rearranging Equation (24) gives the following equation:

$$M = \frac{k_{eq}}{\beta_m (k_{eq} - 2\pi\Delta f \sqrt{\rho l (A_1 + A_2)})^2} - \frac{1}{\beta_m} \tag{25}$$

3. Results and Discussions

In this section, we present the findings of our study on the behavior of DWCNTs with different boundary conditions when subjected to an elastic foundation and a distributed longitudinal magnetic field. First, our results are validated through a comparison with the existing findings in the literature. The natural frequencies of DWCNTs are compared in Table 1. Table 2 presents the natural frequencies of simply supported DWCNTs with different stiffness coefficients. Finally, Table 3 shows the system’s natural frequencies in the presence of the non-local parameter. As shown, the present work agrees with the corresponding results reported by Xu et al. [54], Elishakoff et al. [55], Khosrozadeh et al. [56], and Marmu et al. [57].

Table 1. Natural frequencies ($\times 10^{12}$ Hz) of DWCNTs with different boundary conditions ($d_2 = 1.4$ nm, $d_1 = 0.7$ nm, $\rho = 2300$ kg/m³).

	Elishakoff et al. [55]	Xu et al. [54]	Present Study
simply supported	0.46830	0.46	0.47
cantilevered	0.202	0.17	0.17
bridged	1.0515	1.06	1.085

Table 2. First three natural frequencies ($\times 10^{12}$ Hz) of embedded hinged–hinged DWCNTs with different stiffness coefficients (k) (effective thickness : $h = 34$ nm, $d_1 = 0.684$ nm, $\rho = 2300$ $\frac{kg}{m^3}$).

Mode	$k = 10^8$ N/m ²		$k = 10^9$ N/m ²	
	Khosrozadeh et al. [56]	Present Study	Khosrozadeh et al. [56]	Present Study
1	0.5113	0.4997	0.6665	0.6539
2	1.9328	1.9127	-	1.9571
3	4.1670	4.1817	-	4.2040

Table 3. Natural frequencies ($\times 10^{11}$ Hz) of simply supported DWCNTs with different non-local parameters when outer tube is fixed ($w_2 = 0$) ($d_2 = 1.4$ nm, $d_1 = 0.7$ nm, $\rho = 2300$ $\frac{kg}{m^3}$).

c (TPa)	$e_0 a$ (nm)	Marmu et al. [57]	Present Study
0	0	1.6625	1.6625
	0.5	1.6592	1.6592
	1	1.6496	1.6496
0.0694	0	4.4304	4.4304
	0.5	4.4305	4.4305
	1	4.4846	4.4846

The physical values defined in Table 4 are used for the configuration presented in this section, and the effects of different parameters on sensitivity are investigated in the following plots. The presented model is based on a DWCNT nanoresonator. Figure 2 shows how the magnetic field could affect the frequency shift, decreasing it for the cantilevered nanotube and increasing it for both the simply supported and bridged nanotubes. Increasing the value of the elastic foundation modulus can increase the frequency shift of the simply supported and cantilevered DWCNTs while decreasing the frequency shift of

the bridged DWCNT. Based on Equation (21), the magnetic field contributes to the overall stiffness of the system. Consequently, as the value of H_x increases, its influence on the total stiffness becomes more prominent compared to the other parameters. This is evident when H_x reaches approximately 1.5×10^8 A/m. At this point, the effect of H_x dominates the total stiffness of both cases (with and without mass), and further increases in H_x result in a frequency shift of zero. This observation applies to both the simply supported and the bridged cases. The corresponding diagram converges for all three cases when the magnetic intensity parameter reaches a sufficiently high value.

Table 4. Geometrical and mechanical properties of the nanosensor.

Symbol	Description	Numerical Value
l	Length (nm)	5.55
ρ	Density (kg/m ³)	2300
E	Young's modulus (N/m ²)	1×10^{12}
d_2	Outside diameter (nm)	1.4
d_1	Inside diameter (nm)	0.7
h	Thickness (nm)	0.34
A_2	Outside area (nm ²)	1.4954
A_1	Inside area (nm ²)	0.7477
I_1, I_2	Moments of inertia (nm ⁴)	0.0566, 0.3879
H_x	Magnetic intensity (A/m)	1×10^8
k	Elastic foundation modulus (N/m ²)	5×10^8
ζ	Position of attached mass (nm)	-
M	Attached mass (g)	-
d_2/d_1	Aspect ratio	-
μ	Non-local parameter (nm)	0–1

The effect of the aspect ratio (defined as the ratio of the outer tube diameter to the inner tube diameter) is shown in Figure 3. In all three cases, the aspect ratio has a consistent effect. Higher aspect ratio values result in more remarkable frequency shifts. In the absence of magnetic intensity ($H_x = 0$), the results in this figure align with the findings of Xu et al. [58]. According to their work, in a DWCNT with a greater length, a smaller frequency is observed. This correlation is based on Equation (24), where the frequency shift and frequency are directly related. Furthermore, from a physical perspective, this implies that a larger outer tube diameter in a system with a constant inner tube diameter is more effective in sensing nano-mass, as it exhibits a more significant frequency shift. Similarly, the same effect can be observed in a system with a fixed outer tube diameter where the inner tube has a smaller diameter.

Regarding two systems with equal inner tube diameters but different outer tube diameters, Equation (23) reveals that the system with the larger outer tube diameter has a larger value. This larger value contributes to a smaller second part of Equation (24), resulting in a larger frequency shift. Therefore, the system with the larger outer tube diameter exhibits a greater frequency shift compared to the system with the smaller outer tube diameter. Furthermore, a tube with a higher aspect ratio exhibits greater stiffness than a tube with a smaller one. Consequently, this leads to increases in frequency and mass responsivity, enhancing sensitivity. This observation aligns with the experimental research findings presented by Lassagne et al. [59].

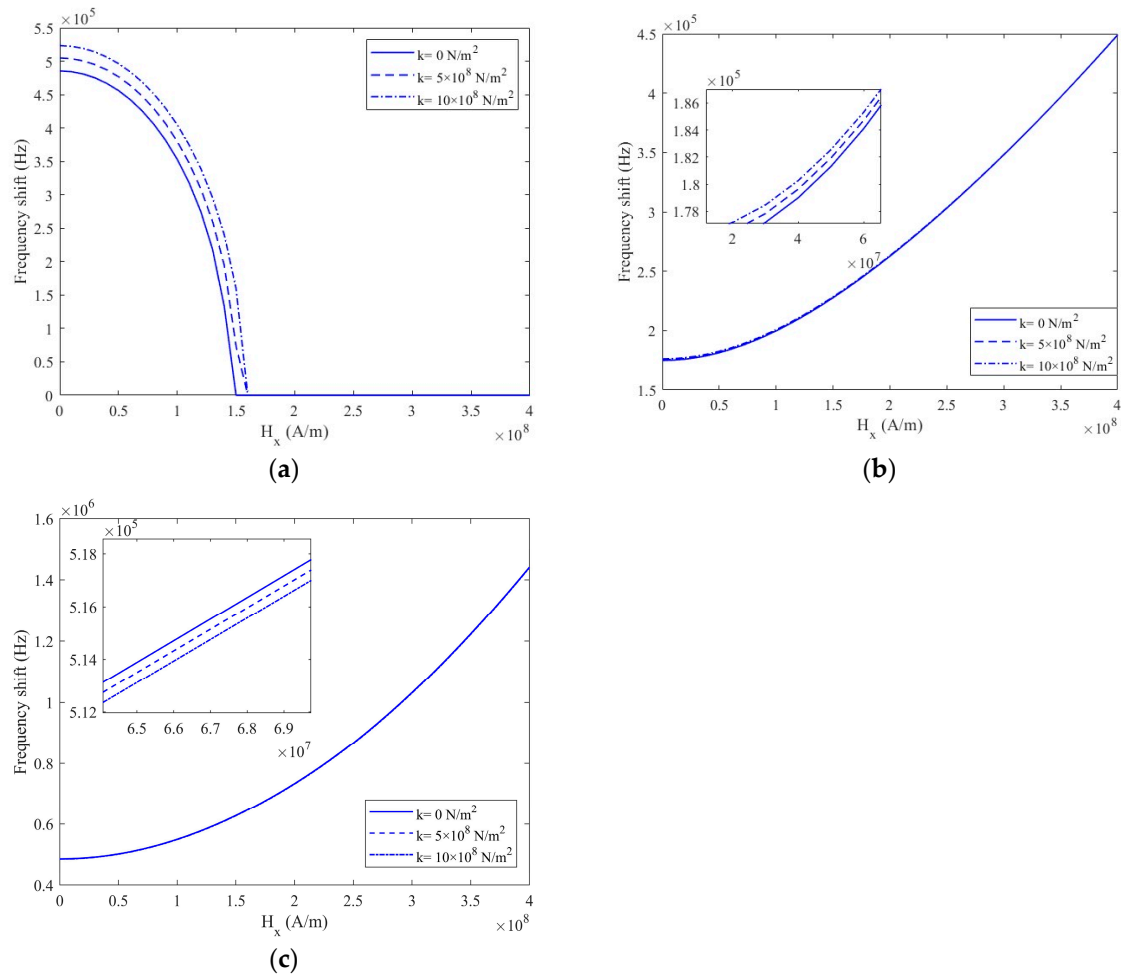


Figure 2. The effect of the magnetic intensity on the frequency shift for various values of the elastic foundation modulus for (a) cantilevered, (b) simply supported, and (c) bridged nanotubes ($\mu = 1 \text{ nm}$).

Furthermore, let us examine why increasing the magnetic intensity causes a more significant divergence among the three aspect ratio cases. It can be attributed to the varying effects of the magnetic field on different systems with different aspect ratios. This difference arises from the direct influence of the surface area on the magnetic force experienced by each system. As the magnetic intensity increases, the impact of the magnetic field becomes more pronounced and distinct for systems with varying aspect ratios. Figure 4 shows the effect of the length ratio (defined as the ratio of the length to the outer tube diameter) on the frequency shift for different boundary conditions. Shorter beams are more sensitive, due to the presence of the magnetic intensity for the bridged, cantilevered, and simply supported nanotubes. In the case of the absence of a magnetic field, this finding is in line with those reported in the literature [11,60] and the experimental observations reported by Chaste et al. [37].

Figure 5 shows how the magnetic intensity can increase or decrease the range of the measurable mass in the three different boundary conditions. As can be seen, larger masses cause greater increases in the frequency shift in the presence of a magnetic field versus its absence for both the simply supported and the bridged nanotubes. However, the frequency shift decreases with increasing magnetic intensity for the cantilevered resonator DWCNTs. The disparity in the behavior of the different systems under the influence of a magnetic field arises from the nature of the magnetic field’s effect on each system’s total stiffness. When a cantilevered system is subjected to a longitudinal magnetic field, the total stiffness decreases, resulting in a stiffer system. Moreover, if we focus solely on the scenario in

which H_x is zero, the pattern observed in the diagram aligns with the results presented by Shen et al. [23].

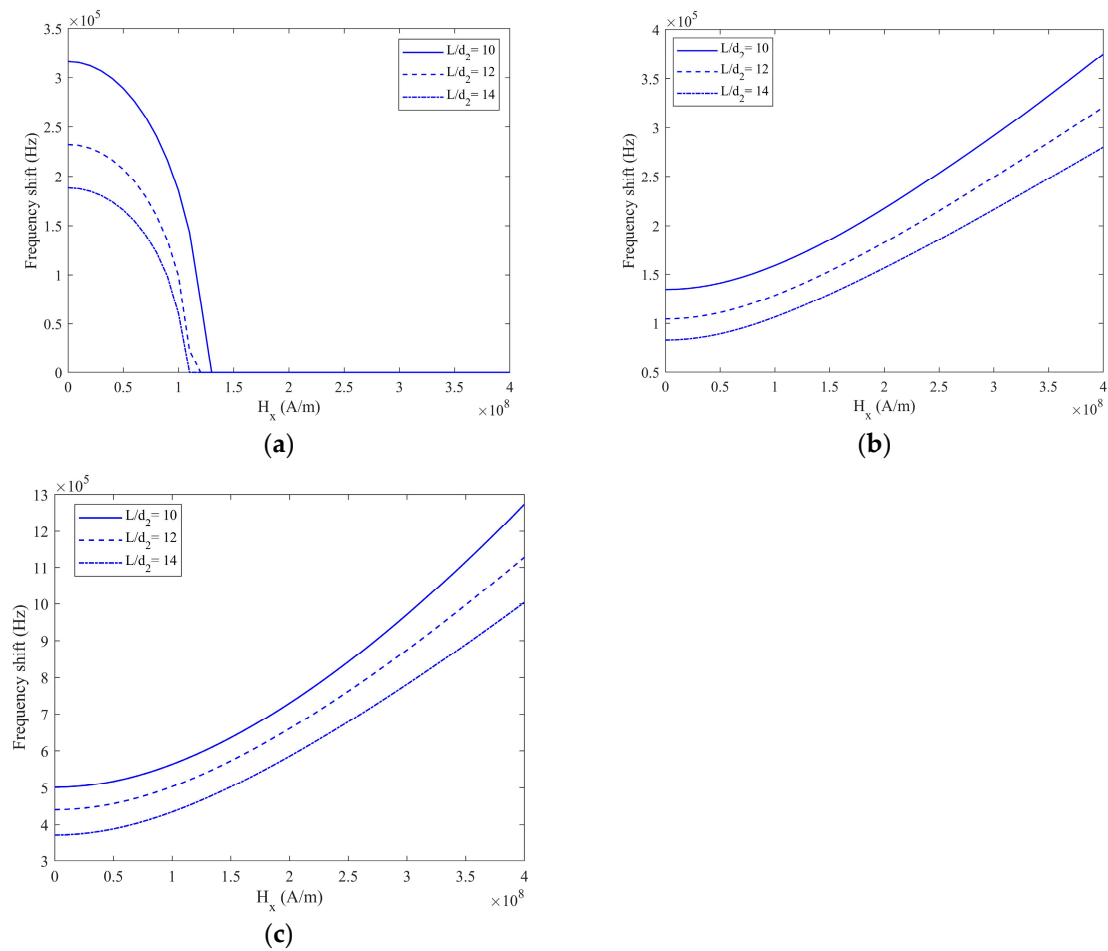


Figure 3. The effect of the magnetic intensity on the frequency shift for various values of the aspect ratio for (a) cantilevered, (b) simply supported, and (c) bridged nanotubes ($\mu = 1$ nm).

Conversely, in the case of the simply supported and bridged systems, the magnetic field makes the systems harder. Consequently, the frequencies of the systems decrease. Then, the frequency shifts decrease based on Equation (24). Therefore, in the presence of a magnetic field, one can potentially obtain higher sensitivity using simply supported and bridged DWCNTs. The observation that a stiffer nanosystem is more capable of sensing mass aligns with the output shown in Figure 4, where smaller nanosystems with higher stiffness are shown to be more effective in capturing small masses.

Finally, Figure 6 shows the effect of the non-local parameter on the frequency shift for the three nanosystems (cantilevered, simply supported, and bridged nanotubes). The non-local parameter decreases the frequency shift for both the simply supported and the bridged nanotubes, while it increases the frequency shift for the cantilevered nanotubes. The effect of non-local parameters is more significant for a bridged nanotube than for the cantilevered and simply supported ones. Here, a connection between the effect of the non-local parameter on the system stiffness and the frequency shift can be made: if the system is stiffer, the frequency shift will be more significant than for a softer system. The effect of the non-local parameter is in agreement with the results published in the literature [61].

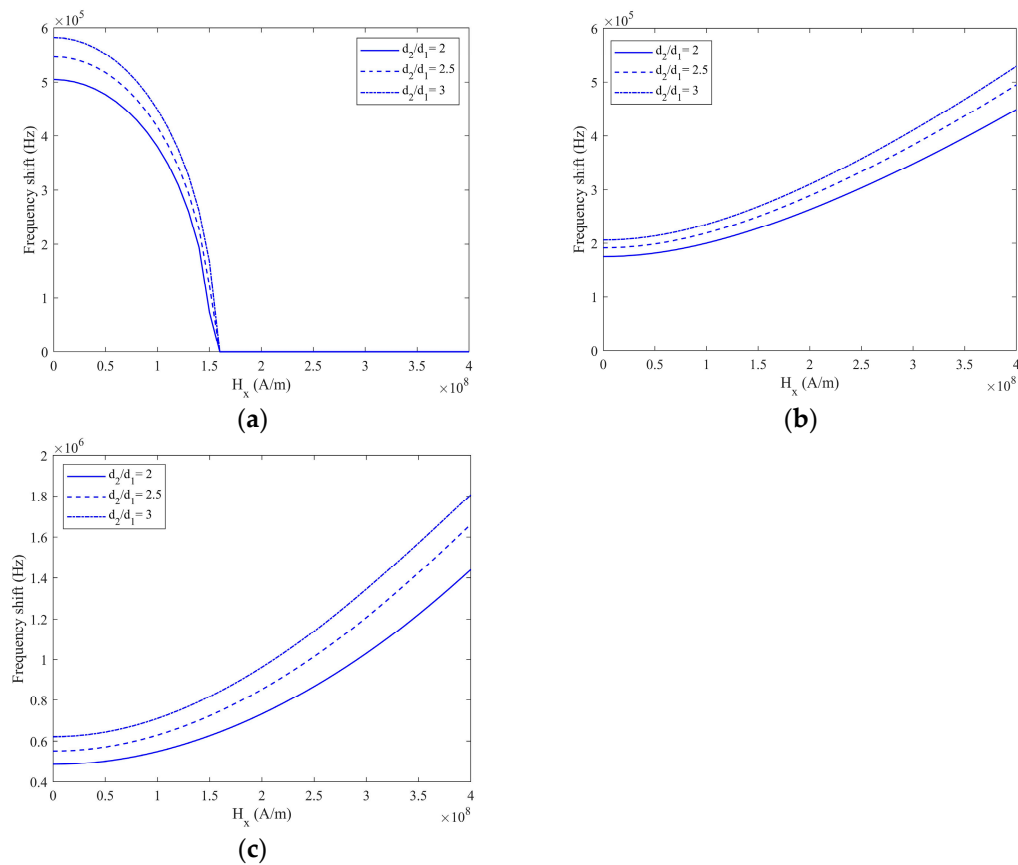


Figure 4. The effect of the magnetic intensity on the frequency shift for various values of length for (a) cantilevered, (b) simply supported, and (c) bridged nanotubes ($\mu = 1 \text{ nm}$, $k = 5 \times 10^8$, $d_2 = 0.7 \text{ nm}$, $\frac{d_2}{d_1} = 2$).

This Study's Limitations and Potential Future Research Areas

As mentioned above, the current study focuses on the possibility of increasing the mass sensitivity of a DWCNT nano-mass sensor using a longitudinal magnetic field. The mass sensitivity of the current model is on the order of 10^{-24} . In comparison to the sensitivity values of some of the other models in the literature, this value is bigger than some and smaller than others. For example, Cho et al. [62] introduced a sensitivity on the order of 10^{-18} for an SWCNT model with a diameter of 2.7 nm and a length of 55 nm. In other works, carried out by Lee et al. [63] for SWCNT models with a diameter of 1.1 nm and lengths of 4.1, 5.6, and 8 nm, the sensitivity was on the order of 10^{-21} . Chaste et al. [64], using a $10 \text{ nm} \times 10 \text{ nm}$ single-layer graphene sheet [65], increased the sensitivity to 10^{-27} . These differences were due to the use of different control parameters, such as geometry, environmental control parameters, temperature, and so on, as mentioned in the introduction. Some of these control parameters are among the limitations of the current model and should be considered when the results of the current model are compared to those in the literature. For example, in the current model, we did not consider the ambient temperature's effect on the nanoresonator's performance, which effectively adds external noise to the system. Meanwhile, the mentioned concept of adding the magnetic field effect to a nano-mass resonator to increase its sensitivity can be extended to other models, such as SWCNTs and nano-beams, due to the similarity of their modeling formulations to those of the current model.

In future work, adding these external control parameters to the model and studying the effect of the magnetic field on the sensor will allow the material of the sensor to be affected by magnetic fields such as those of magnetorheological elastomers.

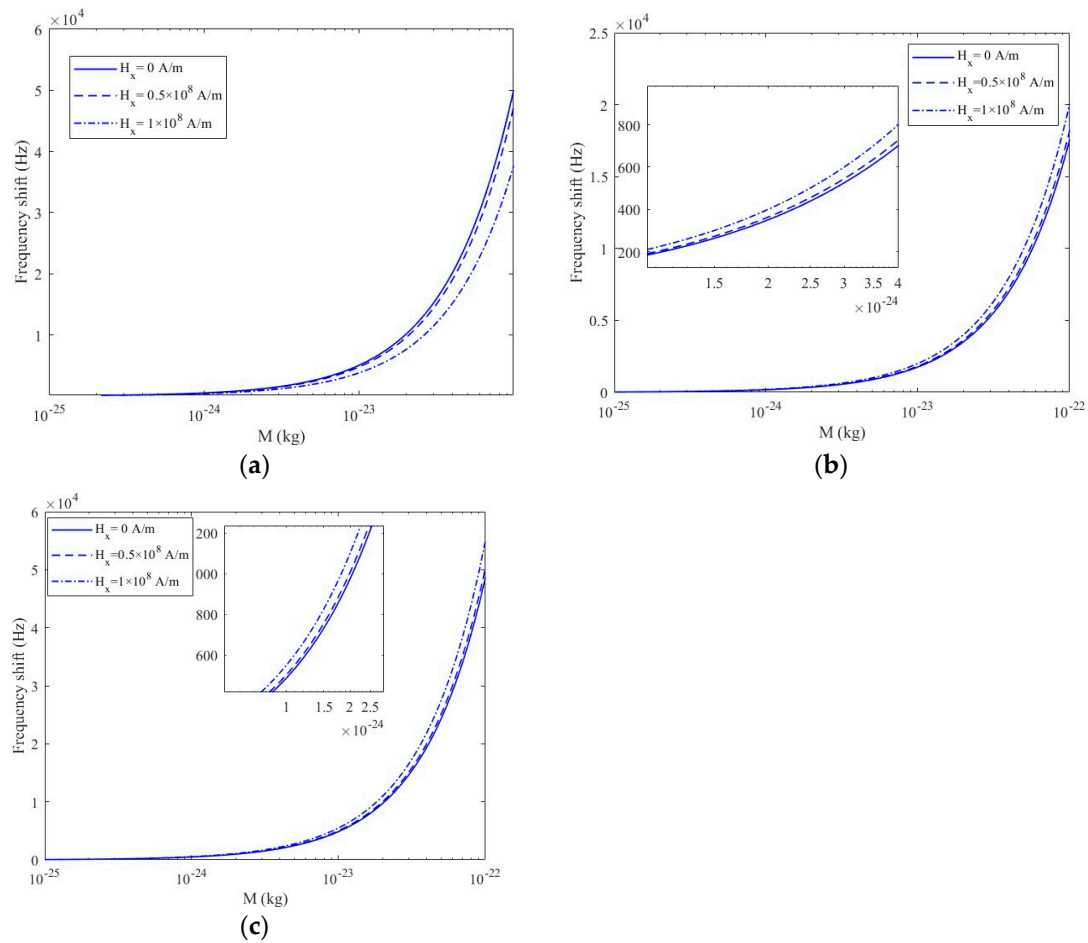


Figure 5. The influence of the longitudinal magnetic field on the sensitivity of DWCNT resonators with (a) cantilevered, (b) simply supported, and (c) bridged nanotubes ($\mu = 1 \text{ nm}$, $k = 5 \times 10^8$).

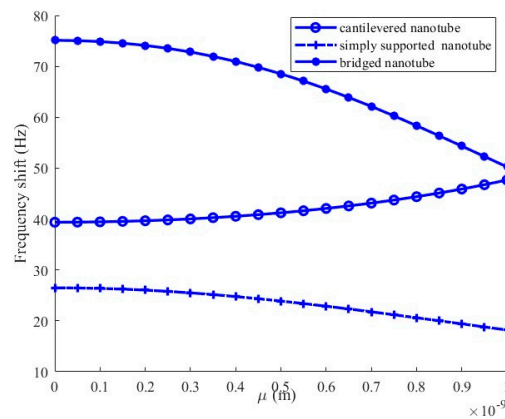


Figure 6. The influence of the longitudinal magnetic field on the sensitivity of DWCNT resonators for the cantilevered, simply supported, and bridged nanotubes ($k = 5 \times 10^8$, $H_x = 1 \times 10^9 \text{ A/m}$).

4. Conclusions

This paper investigated the potential of DWCNTs as nanomechanical mass sensors. The influences of the elastic foundation modulus, length ratio, aspect ratio, magnetic field, and non-local parameters on the frequency shift were explored. The impacts of the different parameters on the frequency shifts of DWCNT resonators with different boundary conditions were presented. It was observed that an increase in the elastic foundation modulus leads to increases in the frequency shift for simply supported and cantilevered

DWCNT resonators and decreases in frequency shift for bridged resonators. Moreover, for simply supported cantilevered and bridged DWCNT resonators, the frequency shift increases significantly when the aspect ratio rises and, for shorter DWCNT lengths, the sensitivity is higher.

Furthermore, the influence of a longitudinal magnetic field on DWCNT resonators varies with their configuration. In cantilevered DWCNT resonators, the field causes a decrease in frequency shift, while it increases the frequency shift in simply supported and bridged resonators. Notably, more pronounced variations in frequency shift for simply supported and bridged DWCNTs were observed with smaller added masses, while opposite effects were observed for the cantilevered configuration. Applying a longitudinal magnetic field enhances the ability of simply supported and bridged DWCNTs to detect smaller masses, which is particularly significant in the case of bridged DWCNTs. This results in more sensitive responses to changes in mass, ultimately increasing the detectability of smaller masses. Although the current study was conducted using a DWCNT nano-mass sensor, the proposed concept (coupling a nano-mass resonator with a magnetic field) can be combined with other models, such as SWCNTs and nano-beam resonators, as the modeling concept is the same for all of these systems. Furthermore, increasing non-local parameters leads to smaller frequency shifts in simply supported and bridged DWCNTs, while the opposite is true for cantilevered systems.

Author Contributions: H.R.A.: methodology, software, visualization, and writing—original draft; Z.R.: conceptualization, methodology, and writing—review and editing; W.S.: methodology and writing—review and editing. All authors have read and agreed to the published version of the manuscript.

Funding: This research received no external funding.

Institutional Review Board Statement: Not applicable.

Informed Consent Statement: Not applicable.

Data Availability Statement: The data supporting the findings of this paper will be made available upon reasonable request.

Conflicts of Interest: The authors declare no conflicts of interest.

References

1. Zhang, X.; Guo, Q.; Cui, D.J.S. Recent advances in nanotechnology applied to biosensors. *Sensors* **2009**, *9*, 1033–1053. [[CrossRef](#)]
2. Kim, W.; Oh, H.; Kwak, Y.; Park, K.; Ju, B.-K.; Kim, K. Development of a carbon nanotube-based touchscreen capable of multi-touch and multi-force sensing. *Sensors* **2015**, *15*, 28732–28741. [[CrossRef](#)] [[PubMed](#)]
3. Chien, W.T.; Chen, C.S.; Chen, H.H. Resonant frequency analysis of fixed-free single-walled carbon nanotube-based mass sensor. *Sens. Actuators A Phys.* **2006**, *126*, 117–121.
4. Schroeder, V.; Savagatrup, S.; He, M.; Lin, S.; Swager, T.M. Carbon nanotube chemical sensors. *Chem. Rev.* **2018**, *119*, 599–663. [[CrossRef](#)] [[PubMed](#)]
5. Kruss, S.; Hilmer, A.J.; Zhang, J.; Reuel, N.F.; Mu, B.; Strano, M.S. Carbon nanotubes as optical biomedical sensors. *Adv. Drug Deliv. Rev.* **2013**, *65*, 1933–1950. [[CrossRef](#)] [[PubMed](#)]
6. Chowdhury, R.; Adhikari, S.; Mitchell, J. Vibrating carbon nanotube based bio-sensors. *Phys. E Low-Dimens. Syst. Nanostruct.* **2009**, *42*, 104–109. [[CrossRef](#)]
7. Trivedi, S.; Kumar, S.; Sharma, S.C.; Harsha, S.P. Biosensing application of multiwall boron nitride nanotube-based nanoresonator for detecting various viruses. *IET Nanobiotechnol.* **2015**, *9*, 259–263. [[CrossRef](#)]
8. Mortimer, M.; Petersen, E.J.; Buchholz, B.A.; Orias, E.; Holden, P.A. Bioaccumulation of multiwall carbon nanotubes in *Tetrahymena thermophila* by direct feeding or trophic transfer. *Environ. Sci. Technol.* **2016**, *50*, 8876–8885. [[CrossRef](#)] [[PubMed](#)]
9. Khater, M.E.; Abdel-Rahman, E.M.; Nayfeh, A.H. A mass sensing technique for electrostatically-actuated mems. In Proceedings of the International Design Engineering Technical Conferences and Computers and Information in Engineering Conference, San Diego, CA, USA, 30 August–2 September 2009; pp. 655–661.
10. Natsuki, T.; Shi, J.-X.; Ni, Q.-Q. Vibration analysis of nanomechanical mass sensor using double-layered graphene sheets resonators. *J. Appl. Phys.* **2013**, *114*, 094307. [[CrossRef](#)]
11. Ardali, J.R.; Ghaderi, R.; Raeiszadeh, F. Effect of microbeam geometry on the nano-mass sensor performance. *Mech. Ind.* **2019**, *20*, 304. [[CrossRef](#)]

12. Gil-Santos, E.; Ramos, D.; Martínez, J.; Fernández-Regúlez, M.; García, R.; San Paulo, Á.; Calleja, M.; Tamayo, J. Nanomechanical mass sensing and stiffness spectrometry based on two-dimensional vibrations of resonant nanowires. *Nat. Nanotechnol.* **2010**, *5*, 641–645. [[CrossRef](#)] [[PubMed](#)]
13. Abadal, G.; Davis, Z.J.; Helbo, B.; Borrise, X.; Ruiz, R.; Boisen, A.; Campabadal, F.; Esteve, J.; Figueras, E.; Perez-Murano, F. Electromechanical model of a resonating nano-cantilever-based sensor for high-resolution and high-sensitivity mass detection. *Nanotechnology* **2001**, *12*, 100. [[CrossRef](#)]
14. Jiang, Y.; Tan, C.Y.; Tan, S.Y.; Wong, M.S.F.; Chen, Y.F.; Zhang, L.; Yao, K.; Gan, S.K.E.; Verma, C.; Tan, Y.-J. SAW sensor for Influenza A virus detection enabled with efficient surface functionalization. *Sens. Actuators B Chem.* **2015**, *209*, 78–84. [[CrossRef](#)]
15. Wasisto, H.S.; Merzsch, S.; Waag, A.; Uhde, E.; Salthammer, T.; Peiner, E. Airborne engineered nanoparticle mass sensor based on a silicon resonant cantilever. *Sens. Actuators B Chem.* **2013**, *180*, 77–89. [[CrossRef](#)]
16. Zarepour, M.; Hosseini, S.A.; Ghadiri, M. Free vibration investigation of nano mass sensor using differential transformation method. *Appl. Phys. A* **2017**, *123*, 181. [[CrossRef](#)]
17. Bouchaala, A.; Nayfeh, A.H.; Younis, M.I. Frequency shifts of micro and nano cantilever beam resonators due to added masses. *J. Dyn. Syst. Meas. Control* **2016**, *138*, 091002. [[CrossRef](#)]
18. Habibi, S.; Nematollahi, M. Position and mass identification in nanotube mass sensor using neural networks. *Proc. Inst. Mech. Eng. Part C J. Mech. Eng. Sci.* **2019**, *233*, 5377–5387. [[CrossRef](#)]
19. Soltani, P.; Pashaei, O.; Taherian, M.M.; Farshidianfar, A. Free vibration of a carbon nanotube-based mass sensor. *Adv. Mater. Res.* **2012**, *403*, 1163–1167. [[CrossRef](#)]
20. Patel, A.M.; Joshi, A.Y. Detection of biological objects using dynamic characteristics of double-walled carbon nanotubes. *Appl. Nanosci.* **2015**, *5*, 681–695. [[CrossRef](#)]
21. Pacholarz, K.J.; Garlish, R.A.; Taylor, R.J.; Barran, P.E. Mass spectrometry based tools to investigate protein–ligand interactions for drug discovery. *Chem. Soc. Rev.* **2012**, *41*, 4335–4355. [[CrossRef](#)]
22. Ghatkesar, M.K.; Barwich, V.; Braun, T.; Ramseyer, J.-P.; Gerber, C.; Hegner, M.; Lang, H.P.; Drechsler, U.; Despont, M. Higher modes of vibration increase mass sensitivity in nanomechanical microcantilevers. *Nanotechnology* **2007**, *18*, 445502. [[CrossRef](#)]
23. Shen, Z.-B.; Tang, G.-J.; Zhang, L.; Li, X.-F. Vibration of double-walled carbon nanotube based nanomechanical sensor with initial axial stress. *Comput. Mater. Sci.* **2012**, *58*, 51–58. [[CrossRef](#)]
24. Herrera-May, A.L.; Soler-Balcazar, J.C.; Vázquez-Leal, H.; Martínez-Castillo, J.; Viguera-Zuñiga, M.O.; Aguilera-Cortés, L.A. Recent advances of MEMS resonators for Lorentz force based magnetic field sensors: Design, applications and challenges. *Sensors* **2016**, *16*, 1359. [[CrossRef](#)]
25. Kumar, A.; Kaur, D. Magnetic field tunable piezoelectric resonator for MEMS applications. *Sens. Actuators A Phys.* **2023**, *364*, 114803. [[CrossRef](#)]
26. White, C.; Piazza, G.; Stephanou, P.; Pisano, A. Design of nano-gap piezoelectric resonators for mechanical RF magnetic field modulation. *Sens. Actuators A Phys.* **2007**, *134*, 239–244. [[CrossRef](#)]
27. Lucklum, F.; Jakoby, B. Novel magnetic–acoustic resonator sensors for remote liquid phase measurement and mass detection. *Sens. Actuators A Phys.* **2008**, *145*, 44–51. [[CrossRef](#)]
28. Murmu, T.; McCarthy, M.; Adhikari, S. Vibration response of double-walled carbon nanotubes subjected to an externally applied longitudinal magnetic field: A nonlocal elasticity approach. *J. Sound Vib.* **2012**, *331*, 5069–5086. [[CrossRef](#)]
29. Sobamowo, M.; Akanmu, J.; Adeleye, O.; Akingbade, S.; Yinusa, A. Coupled effects of magnetic field, number of walls, geometric imperfection, temperature change, and boundary conditions on nonlocal nonlinear vibration of carbon nanotubes resting on elastic foundations. *Forces Mech.* **2021**, *3*, 100010. [[CrossRef](#)]
30. Zhen, Y.-X.; Wen, S.-L.; Tang, Y. Free vibration analysis of viscoelastic nanotubes under longitudinal magnetic field based on nonlocal strain gradient Timoshenko beam model. *Phys. E Low-Dimens. Syst. Nanostruct.* **2019**, *105*, 116–124. [[CrossRef](#)]
31. Sadeghi-Goughari, M.; Jeon, S.; Kwon, H.-J. Effects of magnetic-fluid flow on structural instability of a carbon nanotube conveying nanoflow under a longitudinal magnetic field. *Phys. Lett. A* **2017**, *381*, 2898–2905. [[CrossRef](#)]
32. Zhang, D.; Lei, Y.; Shen, Z. Effect of longitudinal magnetic field on vibration characteristics of single-walled carbon nanotubes in a viscoelastic medium. *Braz. J. Phys.* **2017**, *47*, 640–656. [[CrossRef](#)]
33. Yinusa, A.; Sobamowo, M.; Adelaja, A. Nonlinear vibration analysis of an embedded branched nanofluid-conveying carbon nanotube: Influence of downstream angle, temperature change and two dimensional external magnetic field. *Nano Mater. Sci.* **2020**, *2*, 323–332. [[CrossRef](#)]
34. Arda, M.; Aydogdu, M. Vibration analysis of carbon nanotube mass sensors considering both inertia and stiffness of the detected mass. *Mech. Based Des. Struct. Mach.* **2022**, *50*, 841–857. [[CrossRef](#)]
35. Ceballes, S.; Saunders, B.; Abdelkefi, A. Nonlocal Timoshenko modeling effectiveness for carbon nanotube-based mass sensors. *Eur. J. Mech.-A/Solids* **2022**, *92*, 104462. [[CrossRef](#)]
36. Ekinci, K.; Yang, Y.T.; Roukes, M. Ultimate limits to inertial mass sensing based upon nanoelectromechanical systems. *J. Appl. Phys.* **2004**, *95*, 2682–2689. [[CrossRef](#)]
37. Borm, P.; Klaessig, F.C.; Landry, T.D.; Moudgil, B.; Pauluhn, J.; Thomas, K.; Trottier, R.; Wood, S. Research strategies for safety evaluation of nanomaterials, part V: Role of dissolution in biological fate and effects of nanoscale particles. *Toxicol. Sci.* **2006**, *90*, 23–32. [[CrossRef](#)]

38. Eringen, A.C. On differential equations of nonlocal elasticity and solutions of screw dislocation and surface waves. *J. Appl. Phys.* **1983**, *54*, 4703–4710. [[CrossRef](#)]
39. Mohammadi, F.S.; Rahimi, Z.; Sumelka, W.; Yang, X.-J. Investigation of free vibration and buckling of Timoshenko nano-beam based on a general form of Eringen theory using conformable fractional derivative and Galerkin method. *Eng. Trans.* **2019**, *67*, 347–367.
40. Rahimi, Z.; Sumelka, W.; Baleanu, D. A mechanical model based on conformal strain energy and its application to bending and buckling of nanobeam structures. *J. Comput. Nonlinear Dyn.* **2019**, *14*, 061004. [[CrossRef](#)]
41. Rahimi, Z.; Rezazadeh, G.; Sumelka, W. A non-local fractional stress–strain gradient theory. *Int. J. Mech. Mater. Des.* **2020**, *16*, 265–278. [[CrossRef](#)]
42. Arash, B.; Wang, Q. A review on the application of nonlocal elastic models in modeling of carbon nanotubes and graphenes. In *Modeling of Carbon Nanotubes, Graphene and Their Composites*; Springer: Berlin/Heidelberg, Germany, 2014; pp. 57–82.
43. Ahmadi, H.R.; Rahimi, Z.; Sumelka, W. Thermoelastic damping in orthotropic and isotropic NEMS resonators accounting for double nonlocal thermoelastic effects. *J. Therm. Stress.* **2020**, *44*, 342–358. [[CrossRef](#)]
44. Rashidi, H.; Rahimi, Z.; Sumelka, W. Effects of the slip boundary condition on dynamics and pull-in instability of carbon nanotubes conveying fluid. *Microfluid. Nanofluidics* **2018**, *22*, 131. [[CrossRef](#)]
45. Rahimi, Z.; Yazdani, J.; Hatami, H.; Sumelka, W.; Baleanu, D.; Najafi, S. Determination of hazardous metal ions in the water with resonant MEMS biosensor frequency shift—concept and preliminary theoretical analysis. *Bull. Pol. Acad. Sci. Tech. Sci.* **2020**, *68*, 529–537. [[CrossRef](#)]
46. Rahimi, Z.; Sumelka, W.; Ahmadi, S.R.; Baleanu, D. Study and control of thermoelastic damping of in-plane vibration of the functionally graded nano-plate. *J. Vib. Control* **2019**, *25*, 2850–2862. [[CrossRef](#)]
47. Hutchison, J.; Kiselev, N.; Krinichnaya, E.; Krestinin, A.; Loutfy, R.; Morawsky, A.; Muradyan, V.; Obratsova, E.; Sloan, J.; Terekhov, S. Double-walled carbon nanotubes fabricated by a hydrogen arc discharge method. *Carbon* **2001**, *39*, 761–770. [[CrossRef](#)]
48. Saito, Y.; Nakahira, T.; Uemura, S. Growth conditions of double-walled carbon nanotubes in arc discharge. *J. Phys. Chem. B* **2003**, *107*, 931–934. [[CrossRef](#)]
49. Huang, H.; Kajitara, H.; Tsutsui, S.; Murakami, Y.; Ata, M. High-quality double-walled carbon nanotube super bundles grown in a hydrogen-free atmosphere. *J. Phys. Chem. B* **2003**, *107*, 8794–8798. [[CrossRef](#)]
50. Qiu, H.; Shi, Z.; Guan, L.; You, L.; Gao, M.; Zhang, S.; Qiu, J.; Gu, Z. High-efficient synthesis of double-walled carbon nanotubes by arc discharge method using chloride as a promoter. *Carbon* **2006**, *44*, 516–521. [[CrossRef](#)]
51. Mateiu, R.; Davis, Z.J.; Madsen, D.N.; Møhlhave, K.; Bøggild, P.; Rassmusen, A.-M.; Brorson, M.; Jacobsen, C.J.; Boisen, A. An approach to a multi-walled carbon nanotube based mass sensor. *Microelectron. Eng.* **2004**, *73*, 670–674. [[CrossRef](#)]
52. Amara, K.; Tounsi, A.; Mechab, I. Nonlocal elasticity effect on column buckling of multiwalled carbon nanotubes under temperature field. *Appl. Math. Model.* **2010**, *34*, 3933–3942. [[CrossRef](#)]
53. Pirmoradian, M.; Torhan, E.; Toghraie, D. Study on size-dependent vibration and stability of DWCNTs subjected to moving nanoparticles and embedded on two-parameter foundations. *Mech. Mater.* **2020**, *142*, 103279. [[CrossRef](#)]
54. Xu, K.; Guo, X.; Ru, C. Vibration of a double-walled carbon nanotube aroused by nonlinear intertube van der Waals forces. *J. Appl. Phys.* **2006**, *99*, 064303. [[CrossRef](#)]
55. Elishakoff, I.; Pentaras, D. Fundamental natural frequencies of double-walled carbon nanotubes. *J. Sound Vib.* **2009**, *322*, 652–664. [[CrossRef](#)]
56. Khosrozadeh, A.; Hajabasi, M. Free vibration of embedded double-walled carbon nanotubes considering nonlinear interlayer van der Waals forces. *Appl. Math. Model.* **2012**, *36*, 997–1007. [[CrossRef](#)]
57. Murmu, T.; McCarthy, M.; Adhikari, S. Nonlocal elasticity based magnetic field affected vibration response of double single-walled carbon nanotube systems. *J. Appl. Phys.* **2012**, *111*, 113511. [[CrossRef](#)]
58. Xu, K.-Y.; Aifantis, E.C.; Yan, Y.-H. Vibrations of double-walled carbon nanotubes with different boundary conditions between inner and outer tubes. *J. Appl. Mech. Mar.* **2008**, *75*, 021013. [[CrossRef](#)]
59. Lassagne, B.; Garcia-Sanchez, D.; Aguasca, A.; Bachtold, A. Ultrasensitive mass sensing with a nanotube electromechanical resonator. *Nano Lett.* **2008**, *8*, 3735–3738. [[CrossRef](#)]
60. Li, H.; Wang, X. Nonlinear frequency shift behavior of graphene–elastic–piezoelectric laminated films as a nano-mass detector. *Int. J. Solids Struct.* **2016**, *84*, 17–26. [[CrossRef](#)]
61. Şimşek, M. Large amplitude free vibration of nanobeams with various boundary conditions based on the nonlocal elasticity theory. *Compos. Part B Eng.* **2014**, *56*, 621–628. [[CrossRef](#)]
62. Cho, S.-H.; Choi, M.-S.; Kang, D.-K.; Lee, J.H.; Kim, C.-W. Analysis on mass sensing characteristics of SWCNT-based nano-mechanical resonators using continuum mechanics based finite element analysis. *J. Mech. Sci. Technol.* **2015**, *29*, 4801–4806. [[CrossRef](#)]
63. Lee, H.-L.; Hsu, J.-C.; Chang, W.-J. Frequency shift of carbon-nanotube-based mass sensor using nonlocal elasticity theory. *Nanoscale Res. Lett.* **2010**, *5*, 1774–1778. [[CrossRef](#)] [[PubMed](#)]

64. Chaste, J.; Eichler, A.; Moser, J.; Ceballos, G.; Rurali, R.; Bachtold, A. A nanomechanical mass sensor with yoctogram resolution. *Nat. Nanotechnol.* **2012**, *7*, 301–304. [[CrossRef](#)] [[PubMed](#)]
65. Lee, H.-L.; Yang, Y.C.; Chang, W.J. Mass detection using a graphene-based nanomechanical resonator. *Jpn. J. Appl. Phys.* **2013**, *52*, 025101. [[CrossRef](#)]

Disclaimer/Publisher’s Note: The statements, opinions and data contained in all publications are solely those of the individual author(s) and contributor(s) and not of MDPI and/or the editor(s). MDPI and/or the editor(s) disclaim responsibility for any injury to people or property resulting from any ideas, methods, instructions or products referred to in the content.